Colloid and Interface Science Communications 55 (2023) 100723

Contents lists available at ScienceDirect

Colloid and Interface Science Communications

journal homepage: www.elsevier.com/locate/colcom

Rapid Communication

Cadmium elimination from wastewater using potato peel biochar modified by ZIF-8 and magnetic nanoparticle

Rauf Foroutan [a], Seyed Jamaleddin Peighambardoust [a,*], Solmaz Ghojavand [b], Sima Farjadfard [c], Bahman Ramavandi [c,*]

[a] Faculty of Chemical and Petroleum Engineering, University of Tabriz, Tabriz 5166616471, Iran
[b] Department of Microbiology, Falavarjan Branch, Islamic Azad University, Isfahan, Iran
[c] Department of Environmental Health Engineering, Faculty of Health and Nutrition, Bushehr University of Medical Sciences, Bushehr, Iran

ARTICLE INFO

Keywords:
Potato peel biochar
Nanocomposite
Industrial wastewater
Adsorption
ZIF-8

ABSTRACT

A recyclable and magnetic nanocomposite was fabricated from biochar of potato peel (BPP), $MnFe_2O_4$, and ZIF-8 (BET area: 174.92m^2/g). The Cd^{2+} removal using BPP/$MnFe_2O_4$@ZIF-8 was maximized at pH 6, a temperature of 45 °C, and a time of 100 min. The capacity of Cd adsorption using BPP, BPP/$MnFe_2O_4$, and BPP/$MnFe_2O_4$@ZIF-8 was computed to be 33.76, 45.02, and 80.52 mg/g, respectively. The influence of coexistence ions on cadmium elimination by BPP/$MnFe_2O_4$@ZIF-8 was explored. Shipbuilding wastewater was treated to an acceptable level using the nanocomposite. The Cd adsorption was endothermic and followed the pseudo-second-order ($R^2 > 0.98$). Therefore, BPP/$MnFe_2O_4$@ZIF-8 is an affordable material for treating cadmium.

1. Introduction

Cadmium is a very toxic metal that enters the environment from the wastewater of industries such as electronics. The discharge of cadmium-containing wastewater into the environment is regulated by international organizations due to its high toxicity [1].

Among cadmium elimination methods, surface adsorption has been considered by researchers due to advantages like wide access to different adsorbents, cost-effectiveness, high removal efficiency, and ease of operation [2]. One of the famous adsorbents is biochar, which has characteristics like high carbon, high stability, environmental friendliness, and suitable active surface [3]. The pollutant adsorption capacity of biochar, therefore, its use in wastewater treatment is time-consuming. In this regard, biochar was conditioned by many materials to promote its performance [4,5]. Magnetizing biochar is a method to improve the efficiency of cadmium removal. Magnetic compounds widely affect the physical-chemical properties of biochar and can be easily and quickly isolated from treated solutions [6]. Transition metals or their oxides can be used to produce magnetic compounds, but the use of manganese ferrite nanoparticles ($MnFe_2O_4$) to remove pollutants from aqueous solutions due to high sorption capacity, biocompatibility, chemical stability, and high magnetic sensitivity, high activity surface, presence of active functional groups on its structure, and suitable mechanical resistance has attracted wide attention [7].

Among metal-organic frameworks (MOFs), zeolite imidazolate frameworks-8 (ZIF-8) have been used in many fields [8] and also water and wastewater purification [9] [10–12]. ZIF-8 has a stable structure in ambient air and could eliminate various pollutants through the interaction of H_2 and π-π bonds [13,14]. Modifying biochar with ZIF-8 materials and iron nanoparticles can improve the mass transfer capability and the mechanical structure stability. Further, iron nanomagnet particles make their applicability and separation from the purified solution easier [15].

In this research, the new magnetic composite of BPP/$MnFe_2O_4$@ZIF-8 was applied to remove cadmium (Cd^{2+}) from water and shipyard wastewater. The properties of BPP/$MnFe_2O_4$@ZIF-8 were determined. The RSM-CCD approach was used to investigate the combined impact of effective parameters. The kinetic, thermodynamic, isotherm, reusability, and adsorption mechanism of Cd^{2+} removal were also addressed.

2. Experimental

2.1. Materials

The materials utilized in this research were $Zn(NO_3)_2.6H_2O$ (99%),

* Corresponding authors.
E-mail addresses: j.peighambardoust@tabrizu.ac.ir (S.J. Peighambardoust), b.ramavandi@bpums.ac.ir (B. Ramavandi).

https://doi.org/10.1016/j.colcom.2023.100723
Received 26 March 2023; Received in revised form 30 May 2023; Accepted 31 May 2023
Available online 16 June 2023

2-Methylimidazole (2-MIM, 99%), CH_3OH (≥99.5%), $Cd(NO_3)_2{\cdot}4H_2O$ (≥99% purity), NaOH (99.5%), HCl (37%), $FeCl_3.6H_2O$ (≥98%), and $Mn(NO_3)_2.6H_2O$ (≥99%), which obtained from Merck Co., Germany. Potato peels were collected from local restaurants and used after washing.

2.2. Synthesis of BPP/$MnFe_2O_4$@ZIF-8 nanocomposite

To produce biochar of potato peel (BPP), potato peels were first washed with deionized water and put at 90 °C for 2 days to be fully dried. After drying, the potato peels were heated for 2 h at 500 °C in a thermal oven with a temperature rate of 5 °C/min and under an N_2 gas. After the mentioned time, the prepared biochar was milled and stored in closed containers.

To produce BPP/$MnFe_2O_4$, $FeCl_3.6H_2O$, and $MnCl_2.4H_2O$ were used as precursors in the production of magnetic nanoparticles. For this aim, first, water containing Fe^{3+} and Mn^{2+} with a molar ratio of 2:1 was provided (200 mL). Then, 2 g of biochar was added to it and put in the ultrasonic bath for 50 min. After that, the desired mixture was subjected to continuous stirring at a temperature of 90–95 °C, and 5 M NaOH solution was added (50 mL) and stirred for 3 h. The BPP/$MnFe_2O_4$ was rinsed with deionized water and kept at 105 °C for 1 day.

To modify the BPP/$MnFe_2O_4$ using ZIF-8 metal-organic framework (BPP/$MnFe_2O_4$@ZIF-8), a simple stirring method was used. Briefly, first, 1.5 g of $Zn(NO_3)_2.6H_2O$ was dissolved in 100 mL of CH_3OH, and then 1 g of BPP/$MnFe_2O_4$ was added and agitated for 30 min. Then, 100 mL of methanol solution (3% wt. of 2-MIM) was added to the above mixture and kept under continuous stirring for 24 h at 24 °C. BPP/$MnFe_2O_4$@-ZIF-8 was separated from the methanol solution and placed under vacuum for 24 h at 80 °C to dry. The prepared BPP/$MnFe_2O_4$@ZIF-8 was powdered and tested in the cadmium removal.

2.3. Optimizing the adsorption process using RSM-CCD

This section is presented in the Supplementary section (including Table S1 and Table S2 in the Supplementary Information section).

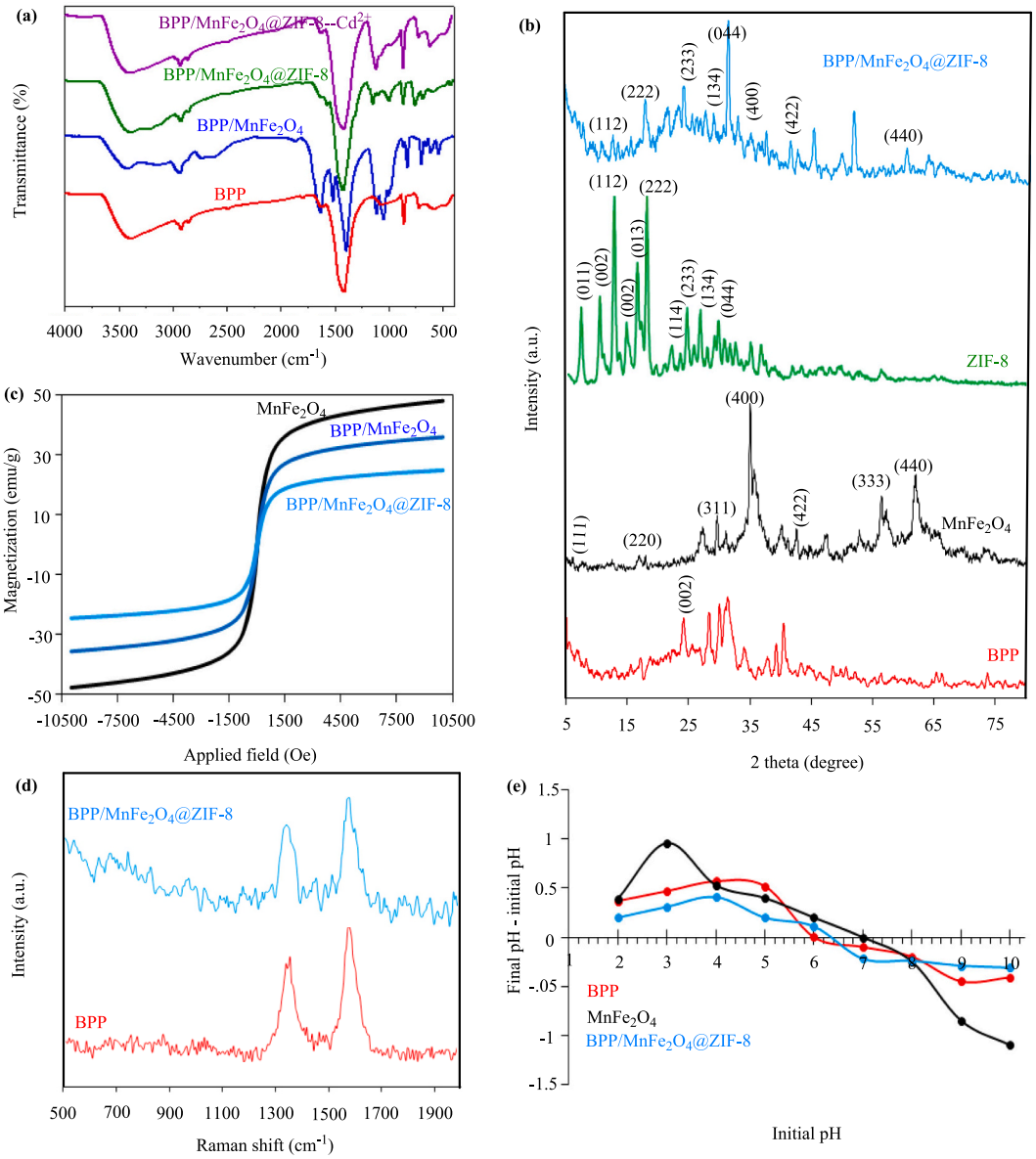

Fig. 1. (a) FTIR for fresh sample (BPP/$MnFe_2O_4$@ZIF-8) and their components (BPP and BPP/$MnFe_2O_4$) and used sample (BPP/$MnFe_2O_4$@ZIF-8-Cd^{2+}), (b) XRD for fresh samples (BPP, $MnFe_2O_4$, ZIF-8, and BPP/$MnFe_2O_4$), (c) VSM for magnetized samples ($MnFe_2O_4$, BPP/$MnFe_2O_4$, and BPP/$MnFe_2O_4$), (d) Raman analysis for the biochar-contained samples (BPP and BPP/$MnFe_2O_4$), and (e) 'Final pH-initial pH' against initial pH for determination zero point charge (pHzpc).

3. Results and discussion

3.1. Properties of adsorbents

The FTIR spectrum for fresh and utilized BPP, BPP/$MnFe_2O_4$, and BPP/$MnFe_2O_4$@ZIF-8 is shown in Fig. 1a. In the wavenumbers of 3384–3419 cm^{-1}, a broad peak has appeared in the samples, which can be caused by -OH [16]. In the desired samples, a low-intensity peak was observed at 2854–2927 cm^{-1}, which can be attributed to C—H [16]. Vibrations with different intensities have been observed at 1797, 1629–1629, 1415–1420, and 1047–1100 cm^{-1}, which are related to C═O functional groups, amides (carbonyl stretching vibrations in peptide bonds) [16], C—H, and C-O-C [17], respectively. Vibrations have appeared in BPP (at 720–863 cm^{-1}) are attributed to C—H vibrations. After modification of BPP using $MnFe_2O_4$ and ZIF-8 magnetic nanoparticles, new absorption peaks have observed at 594 and 426 cm^{-1}, which are related to Fe—O in $MnFe_2O_4$ and Zn—N in ZIF-8, respectively [17]. In addition, after modification of BPP using magnetic nanoparticles $MnFe_2O_4$ and ZIF-8, the situation of C—H in BPP changed from 1415 to 1393 and 1420 cm^{-1}, respectively, which could be corresponded to the interaction of magnetic $MnFe_2O_4$ and 2-MIM rings with BPP [18]. Change or disappearance of some absorption peaks after Cd^{2+} removal can correspond to the interaction and coverage of functional groups by Cd^{2+}.

The XRD findings are shown in Fig. 1b. In BPP, a broad peak has appeared at $2\theta = 23.9^{\circ}$, which is attributed to the crystalline phases (002) of the hexagonal lattice of graphite layers [19]. In addition, different peaks have appeared in BPP in the ranges of 20–45°, which can be caused by $MgCO_3$, $CaCO_3$, $Ca_3(PO_4)_2$, and CaO [20]. In $MnFe_2O_4$, peaks have appeared at 5–80°, indicating the presence of crystal phases (111), (220), (311), (400), (422), (333), and (440) in the desired nanoparticle structure [21]. Also, in ZIF-8, peaks have appeared at 5–30°, which shows the existence of different crystal phases that confirm the successful synthesis of ZIF-8 [13]. After the formation of the BPP/$MnFe_2O_4$@ZIF-8, a peak related to BPP, $MnFe_2O_4$, and ZIF-8 appeared, which shows that the desired magnetic nanocomposite has been generated and the constituents have an interaction with each other.

Vibrating sample magnetometer (VSM) analysis was conducted to explore the behavior and magnetic properties of $MnFe_2O_4$, BPP/$MnFe_2O_4$, and BPP/$MnFe_2O_4$@ZIF-8 samples and the findings are shown in Fig. 1c. As the findings show, the saturation value of magnetism for the samples of $MnFe_2O_4$, BPP/$MnFe_2O_4$, and BPP/$MnFe_2O_4$@ZIF-8 were determined to be 47.83, 35.74, and 24.66 emu/g, respectively. In addition, the results showed that the magnetic saturation value for BPP/$MnFe_2O_4$@ZIF-8 is lower compared to the other two materials, which is caused by the presence of non-magnetic particles of BPP and ZIF-8. Nevertheless, the determined magnetic saturation value ensures that the BPP/$MnFe_2O_4$@ZIF-8 can be separated from the water media in <2 min [22], which is an encouraging result for the rapid separation and reuse of the BPP/$MnFe_2O_4$@ZIF-8 magnetic nanocomposite in the field of wastewater works. Further, the obtained VSM spectrum for all three samples has the coercive force and magnetization remanence, which indicates the superparamagnetic properties of the samples [23].

Raman spectroscopy for samples of BPP and BPP/$MnFe_2O_4$@ZIF-8 has been performed at 500–2000 cm^{-1} to investigate the graphite structure and the interaction between the components of the magnetic nanocomposite structure (Fig. 1d). In the structure of BPP, two peaks with high intensity have appeared at 1361 and 1582 cm^{-1}, which show D (disordered carbon atom, sp^3) and G (corresponding to an ordered carbon atom, sp^2) bands, respectively [24]. The range of D and G peaks in the BPP structure changed to 1332 and 1574 cm^{-1}, respectively, after modification using $MnFe_2O_4$ and ZIF-8, which can be caused by the placement of $MnFe_2O_4$ and ZIF-8 in BPP. Also, in the Raman spectrum of BPP/$MnFe_2O_4$@ZIF-8 magnetic nanocomposite in the range of 500-1000 cm^{-1} and 1400 cm^{-1}, peaks were observed that were not present in the BPP structure. These peaks can be caused by E_g, T_{2g}, and A_{1g} states of inverted spinel compounds in the structure of $MnFe_2O_4$ [21] and ZIF-8 [25].

The solution pH affects the concentration of surface charges of the adsorbent, and consequently the efficiency of the adsorption process. Therefore, the positive or negative surface charge of adsorbents at different pH should be determined. For this purpose, pHzpc is required, the results of which are shown in Fig. 1e. Based on the results, the value of pHzpc for BPP, $MnFe_2O_4$, and BPP/$MnFe_2O_4$@ZIF-8 samples was determined to be 6.04, 7, and 6.38 respectively, which shows that the mentioned samples have negative and positive charges at solution pHs higher and lower than pHzpc, respectively.

N_2 adsorption-desorption isotherms at 77 K were investigated to determine the specific surface, pores volume, and pores diameter of BPP, ZIF-8, BPP/$MnFe_2O_4$, and BPP/$MnFe_2O_4$@ZIF-8 magnetic nanocomposite (Fig. S1). The value of the specific surface area for BPP, ZIF-8, BPP/$MnFe_2O_4$, and BPP/$MnFe_2O_4$@ZIF-8 was 1.40, 1063.6, 109.35, and 174.92m^2/g, respectively. It was determined that the presence of $MnFe_2O_4$ and ZIF-8 nanoparticles improved the surface area of BPP. Also, the average pore diameter for BPP has calculated at 103.27 nm, which confirms that BPP is macroporous, while the average pore diameter in ZIF-8 was computed at 1.63 nm, which reveals the very few mesoporous natures of ZIF-8. ZIF-8 has a microporous structure in previous studies [13]. After modification of BPP by using magnetic nanoparticles $MnFe_2O_4$ and ZIF-8, the pores in BPP changed from macropore to mesoporous, which indicates that magnetic nanoparticles $MnFe_2O_4$ and ZIF-8 were embedded on BPP. The results showed that the modification of BPP using BPP/$MnFe_2O_4$ magnetic nanoparticles and ZIF-8 improved the pores volume in BPP. Based on the nitrogen adsorption-desorption isotherm and the IUPAC standard, BPP, ZIF-8, BPP/$MnFe_2O_4$, and BPP/$MnFe_2O_4$@ZIF-8 are belonged to type II [26], type I [27], type IV, and type IV [28], respectively.

SEM-EDX and dot-mapping tests are shown in Fig. S2. Based on the results, there are large pores on the surface of the BPP sample (Fig. S2A), which is in good agreement with the BET results and confirms the existence of the macropore structure of the BPP sample. In addition, in the structure of BPP, there are elements of carbon, oxygen, phosphorus, and calcium, most of which is carbon (Fig. S2B—C) and it shows that BPP is composed of graphite layers and is consistent with the results of Raman analysis. After modifying BPP using $MnFe_2O_4$, particles of different sizes appeared on the BPP surface and the macropores in BPP almost disappeared, which could be due to the placement of $MnFe_2O_4$ magnetic nanoparticles in the macropores (Fig. S2D). To confirm the formation of $MnFe_2O_4$ in the BPP structure, Map-EDX analyses confirmed the presence of Mn and Fe elements in BPP (Fig. S2E—F). BPP/$MnFe_2O_4$ magnetic nanocomposite was modified using ZIF-8 to improve the active surface and its performance. The results of SEM and Map-EDX showed that after the modification process, the density of particles in the BPP/$MnFe_2O_4$ surface has increased, and there are also zinc and nitrogen elements (2-methylimidazole rings) in its structure, which confirms the presence of ZIF-8. These results are consistent with the findings of XRD and BET tests (Fig. S2G—I). After the Cd^{2+} removal using BPP/$MnFe_2O_4$/ZIF-8, particles with larger sizes and higher density appeared on the surface of the desired magnetic nanocomposite (Fig. S2J). To confirm the ability of the magnetic nanocomposite to adsorb Cd^{2+}, Map-EDX analysis was also used, which confirmed the existence of Cd^{2+} in the sample (Fig. S2K-L) and showed that BPP/$MnFe_2O_4$/ZIF-8 has the suitable ability for adsorbing Cd^{2+} and can be used as an effective adsorbent.

3.2. RSM-CCD analysis

This part has been presented in the Supplementary Section (including Table S2, Table S3, Fig. S2, and Fig. S3).

3.3. Influence of parameters

Based on Fig. 2, all studied parameters are effective in cadmium decontamination. The results showed that the adsorption efficiency of Cd^{2+} increased with the increase of treatment time from 20 to 100 min, which can be due to the existence of enough time for Cd^{2+} to be placed on the BPP/$MnFe_2O_4$@ZIF-8.

The cadmium removal increased by raising the pH level from 2 to 6 and then declined. The low yield value at pH 2 can be caused by the high amount of H^+, which competes with the cadmium ion to occupy the active sites (pH < pHzpc). When the pH increases from 2 to 6, H^+ decrease, and the density of positive charges on the surface of the adsorbent decreases. As a result, the competition between Cd^{2+} and H^+ decreases, and a sufficient surface is provided for the Cd^{2+} decontamination (pH = pHzpc). After pH 6 (pH > pHzpc), the level of negative charge (OH^-) in the water media increases, and between Cd^{2+} and the negative charge, the adsorption rate decreases, which can be caused by the interaction between Cd^{2+} and OH^- and the formation of a complex $Cd(OH)_2$ and precipitation of Cd^{2+} [29]. Therefore, pH 6 with a removal efficiency of 99.32% was determined as the optimum value.

The results of 3D response surface graphs (Fig. 2) and 2D graphs (Fig. S4) to investigate the effect of parameters individually showed that increasing the temperature has increased the Cd adsorption, indicating that the adsorption is endothermic. This phenomenon can be caused by the decrease in the boundary layer thickness around the composite and the increase in the penetration rate of Cd^{2+} on the adsorbent and the increase of suitable and available sites for the adsorption of cadmium [30]. The effect of the Cd^{2+} concentration was investigated (Fig. 2 and Fig. S4). The maximum efficiency has been achieved at 10 mg/L, and with the increase of the Cd concentration, the removal rate has decreased. The high efficiency at 10 mg/L compared to 50 mg/L can be due to the presence of active sites to absorb Cd^{2+} [30]. The adsorbent dose was assessed and the findings showed that the removal rate had an increasing trend in the desired mass of 0.4–1 g/L, however, after that, the efficiency decreased. The increasing trend can be due to the availability of surface and unsaturated sites to absorb Cd^{2+}. According to Fig. S4, optimal values of temperature, adsorption time, adsorbent mass, Cd^{2+} concentration, and pH were determined as 45 °C, 100 min, 1 g/L, 10 mg/L, and 6, respectively.

3.4. Kinetic study

The curve of the kinetic models is presented in Fig. 3 and the kinetic rate and correlation coefficient (R^2) are listed in Table S4. Based on the results, the R^2 number of the pseudo-second-order (PSO) is higher than other models, which shows that PSO has a more appropriate model to describe the behavior of the adsorption. The adopting of the kinetic behavior of the adsorption process from the PSO model shows that the adsorption of Cd^{2+} is chemical, electrostatic, and chelate surface adsorption, and the reactions on the surface may be limit the speed of the process and govern the adsorption mechanism of Cd^{2+} [19]. It should be noted that the value of the adsorption constant rate (k_1,k_2) determined for the adsorption process using BPP/$MnFe_2O_4$@ZIF-8 is higher compared to other used adsorbents, which can be caused by the active surface, high and its microporous structure [30]. This finding is inconsistent with those obtained in the BET test. Also, the α value showed that the adsorption ability of BPP/$MnFe_2O_4$@ZIF-8 magnetic nanocomposite in adsorbing Cd^{2+} is higher compared to other adsorbents. Based on this model, the chemical mechanisms support the cadmium adsorption onto the adsorbents [7]. In the intra-particle diffusion (IPD) model, the depicted lines for q_t *vs.* $t^{0.5}$ did not cross the origin, showing that more than one type of mechanism (intra-particle diffusion, boundary layer effect) is involved in the process.

3.5. Isotherm study

To explore the equilibrium behavior of the Cd^{2+} removal, adsorption experiments were conducted (Fig. S5a). The nonlinear regression of the isotherm models is shown in Fig. S5b-d and the parameters are reported in Table 1. In the Cd^{2+} adsorption using BPP and BPP/$MnFe_2O_4$ samples, the R^2 parameter of the Langmuir is bigger than in other models, which means that the removal of cadmium occurs in multilayer on the heterogeneous surface of the adsorbents. While in the adsorption of Cd^{2+} using BPP/$MnFe_2O_4$@ZIF-8, the data followed the Freundlich isotherm and the adsorption was monolayer on the homogeneous surface of the composite. The higher value of Langmuir K_L indicates the affinity of the adsorbent to cadmium, which BPP/$MnFe_2O_4$@ZIF-8 has the highest value among other studied materials in this study. In addition, in the Cd adsorption by all studied adsorbents, $0 < R_L \langle 1,n \rangle 1$, and $E < 8$ kJ/mol, which show that the process is favorable and physical. The amount of adsorption capacity for BPP, BPP/$MnFe_2O_4$, and BPP/$MnFe_2O_4$@ZIF-8 was determined to be 33.76, 45.02, and 80.52 mg/g, respectively, and the high adsorption capacity of BPP/$MnFe_2O_4$@ZIF-8 compared to other samples can be caused by specific surface and high adsorption bond energy [11]. The Temkin isotherm showed that physical adsorption can also play a role in the Cd^{2+} removal using adsorbents.

3.6. Thermodynamic study

Examining the effect of temperature (Fig. 4a) showed that the adsorption of Cd^{2+} using BPP and BPP/$MnFe_2O_4$@ZIF-8 is endothermic. To determine ΔG°, ΔH°, and ΔS°, the van't Hoff equation was used and the linear relationship of $\ln K_C$ *versus* 1/T is shown in Fig. 5b.

Based on Table S5, the value of ΔG° for both adsorbents (BPP and BPP/$MnFe_2O_4$@ZIF-8) was negative, which shows that the Cd^{2+} elimination using the desired adsorbents is physical. The values of ΔH° and ΔS° parameters for the Cd^{2+} removal using BPP were 26.03 kJ/mol and 103.55 J/mol.K, respectively, and using BPP/$MnFe_2O_4$@ZIF-8 were determined 37.653 kJ/mol and 497.211 J/mol.K, respectively. The value shows that the desired surface adsorption is endothermic and the random collisions between Cd^{2+} and adsorbents have increased, and increasing the temperature favors the spontaneous adsorption process [11].

3.7. Counter ions effect and reusability

The presence of Na^+, K^+, and Ca^{2+} in the water media reduced the Cd^{2+} removal, which can be caused by the saturation of the active sites and intensified competition between these ions with Cd^{2+} (Fig. S6a-c). In addition, Na^+, K^+, and Ca^{2+} have a positive charge, which, if placed on the adsorbent, causes the electrostatic force of repulsion with Cd^{2+}, and as a result, the efficiency of the process decreases. Another noteworthy point is that sodium, potassium, and calcium ions had a greater inhibitory effect on cadmium adsorption by BPP than BPP/$MnFe_2O_4$@ZIF-8. This indicates the complexity of the functional groups and the greater surface area of the BPP/$MnFe_2O_4$@ZIF-8 composite.

The reusability of BPP and BPP/$MnFe_2O_4$@ZIF-8 in the Cd^{2+} adsorption of up to 8 steps was investigated (Fig. S6d). The findings showed that BPP/$MnFe_2O_4$@ZIF-8 compared to BPP has a high ability to remove Cd^{2+} and up to 8 stages of reuse, its adsorption efficiency is >90%, while the adsorption efficiency of the BPP after 4 steps decreased to <90%. The ability of BPP/$MnFe_2O_4$@ZIF-8 in adsorbing Cd^{2+} can be related to the high BET surface and the presence of effective functional groups.

3.8. Cd^{2+} adsorption mechanisms

The removal mechanism of metal ions using biochar usually includes surface complexation, metal ion exchange, Cd-π interaction, physical surface adsorption, and co-precipitation. One of the effective

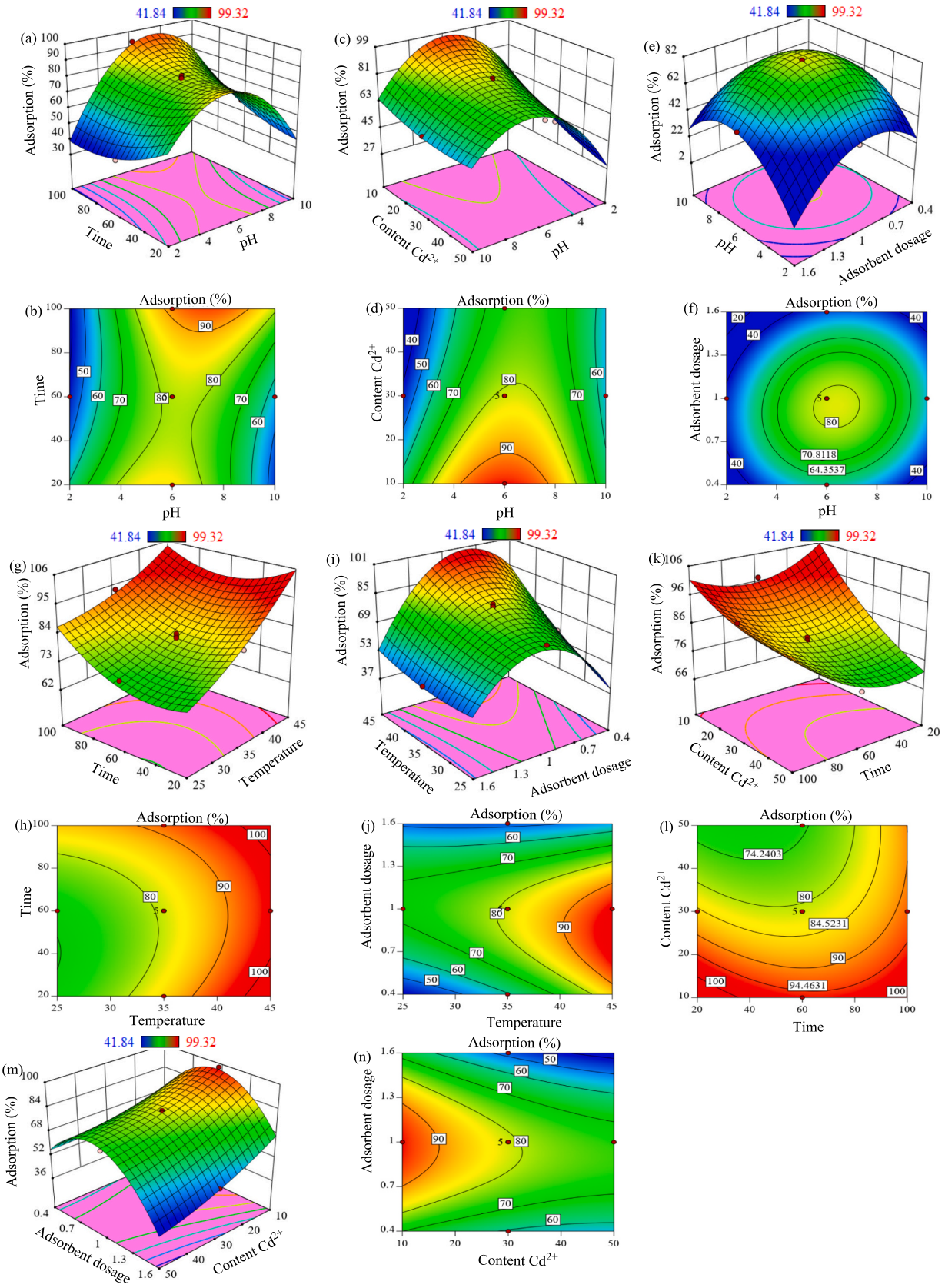

Fig. 2. 3D and 2D graphs to investigate the effect of (a,b) pH and contact time, (c,d) pH and Cd^{2+} concentration, (e,f) pH and adsorbent dose, (g,h) contact time and temperature, (I,j) temperature and adsorbent dose (*k*,*l*) Cd^{2+} concentration and contact time, (m,n) contact time and Cd^{2+} concentration on the adsorption efficiency using BPP/$MnFe_2O_4$@ZIF-8.

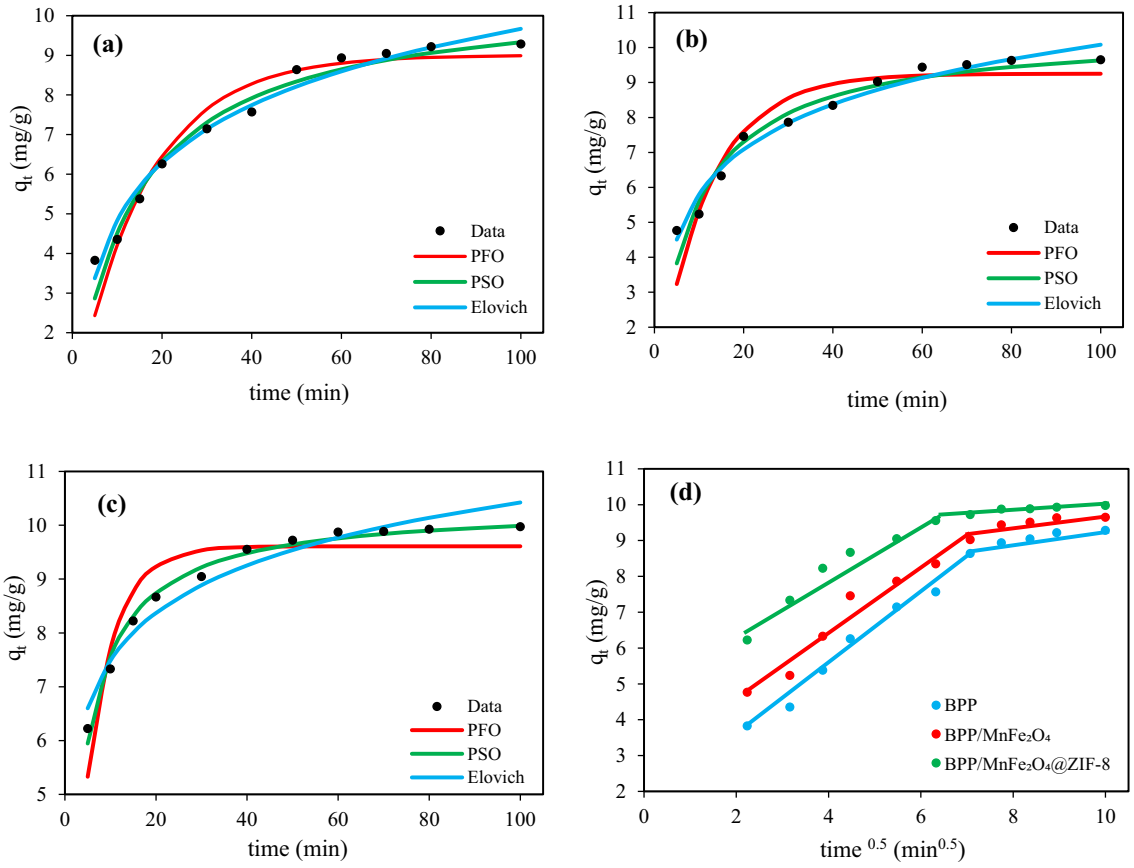

Fig. 3. Non-linear kinetic models for Cd^{2+} removal using (a) BPP, (b) BPP/$MnFe_2O_4$, and (c) BPP/$MnFe_2O_4$@ZIF-8 and (d) the intra-particle diffusion model for Cd^{2+} removal using the desired samples.

Table 1
The results of equilibrium parameters.

Isotherm model	Adsorbent			Isotherm model	Adsorbent		
	BPP	BPP/$MnFe_2O_4$	BPP/$MnFe_2O_4$@ZIF-8		BPP	BPP/$MnFe_2O_4$	BPP/$MnFe_2O_4$@ZIF-8
Langmuir				D-R			
q_m(mg/g)	33.76	45.02	80.52	E(kJ/mol)	1.385	1.717	2.405
K_L(L/mg)	0.5864	0.7064	1.224	q_m(mg/g)	30.32	39.12	52.63
R_L	0.021–0.145	0.017–0.124	0.010–0.075	β(mol^2/J^2)	2.604×10^{-7}	1.695×10^{-7}	8.642×10^{-8}
Adj R^2	0.9941	0.973	0.8794	Adj R^2	0.932	0.8813	0.7338
RMSE	0.6872	2.192	6.687	RMSE	2.337	4.596	9.933
R^2	0.995	0.9769	0.8966	R^2	0.9418	0.8982	0.7718
Freundlich				Temkin			
n	4.468	3.836	3.64	b_T(kJ/mol)	0.508	0.361	0.348
K_f (mg/g(L/mg)$^{1/n}$)	15.13	19.32	30.51	A_T(L/g)	11.3	10.99	75.49
Adj R^2	0.859	0.9016	0.8972	Adj R^2	0.8912	0.9617	0.9328
RMSE	3.367	4.185	2.177	RMSE	0.9349	2.611	4.992
R^2	0.8791	0.9156	0.989	R^2	0.9442	0.9672	0.9424

mechanisms in the process of adsorption is the electrostatic force created between the active groups in the adsorbent with desired pollutants. FTIR analysis (Fig. 1a) showed that there are –OH, C═O, C—H, C-O-C, N—H, Zn—N, and C═C in the magnetic nanocomposite structure (2-MIM structure). These mentioned functional groups can interact with Cd^{2+} in the water media and remove it through complexation and cation-π interaction mechanisms [15]. In addition to the mentioned functional groups, another effective mechanism that can be effective in removing Cd^{2+} are the mechanism of cation exchange and chemical precipitation (Fig. 5). EDX and XRD analyses proved that there are various cations such as Mg^{2+}, Ca^{2+}, K^+, and P (PO_4^{3-}) in the BPP. The mentioned anions and cations can be released from the BPP surface and interact with Cd^{2+} and remove it from the water through chemical precipitation mechanisms ($CdCO_3$, $Cd_3(PO_4)_2$) and cation exchange [15]. There are also Fe^{3+}, Mn^{2+}, and Zn^{2+} in the BPP/$MnFe_2O_4$@ZIF-8 structure that can be effective in the ion exchange mechanism. The area and pores of the adsorbent are also vital in cadmium adsorption. BET and SEM tests showed that in the constituent components of BPP/$MnFe_2O_4$@ZIF-8, there are pores (with different sizes and diameters) that can remove Cd^{2+} through the process of van der Waals forces.

3.9. Industrial wastewater treatment

The wastewater treatment process of the shipbuilding industry was

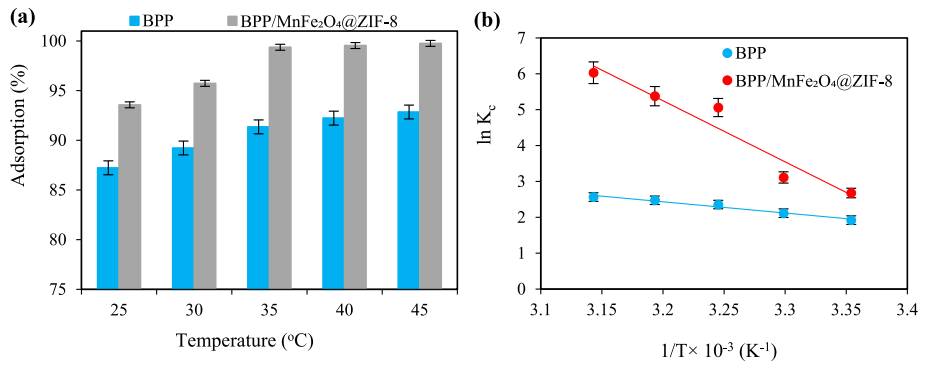

Fig. 4. (a) The temperature effect (adsorbent: 1 g/L, pH: 6, time: 100 min, Cd^{2+}: 10 mg/L, n = 3) and (b) Van't Hoff's linear relationship for determination thermodynamic parameters (n = 3).

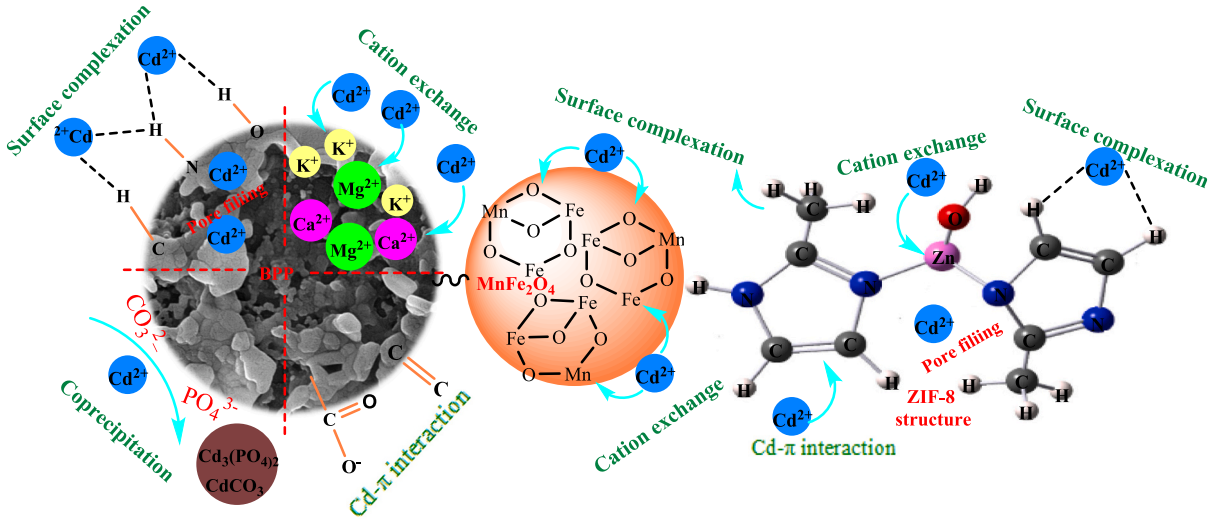

Fig. 5. Mechanisms of Cd^{2+} removal by BPP/$MnFe_2O_4$@ZIF-8.

carried out under optimal parameters. The metal ions concentration in the wastewater of the shipbuilding industry after the cleaning process was significantly reduced (Table S6). The final pH of treated wastewater was slightly increased and closed to neutral. This shows that the nanocomposite adsorbent has amphoteric properties. The high ability of BPP/$MnFe_2O_4$@ZIF-8 in removing metal ions in shipbuilding industry wastewater revealed that the magnetic nanocomposite can be utilized as a vital alternative in wastewater treatment.

3.10. Comparison of adsorption capacity

The results of this study have been compared with other studies (see Table S7) and it confirms the superiority of the adsorbent of this study compared to other adsorbents.

4. Conclusions

The BPP/$MnFe_2O_4$@ZIF-8 (porous, crystalline, mesopore, and magnetic material) was used for cadmium removal from wastewater. The effect of parameters was explored using RSM-CCD. The cadmium adsorption data followed the PSO kinetic. In the Cd^{2+} adsorption using BPP/$MnFe_2O_4$@ZIF-8, the heterogeneous surface had a more effective role. The adsorption process was spontaneous and endothermic during the process. The wastewater of the shipbuilding industry was treated by the developed adsorbent. The BPP/$MnFe_2O_4$@ZIF-8 can be reused several times, so this is an economic and vital composite.

CRediT authorship contribution statement

Rauf Foroutan: Formal analysis, Methodology. **Seyed Jamaleddin Peighambardoust:** Methodology, Supervision. **Solmaz Ghojavand:** Methodology. **Sima Farjadfard:** Methodology, Conceptualization. **Bahman Ramavandi:** Supervision, Conceptualization, Methodology, Writing – review & editing.

Declaration of Competing Interest

The authors declare that they have no known competing financial interests or personal relationships that could have appeared to influence the work reported in this paper.

Data availability

Data will be made available on request.

Appendix A. Supplementary data

Supplementary data to this article can be found online at https://doi.org/10.1016/j.colcom.2023.100723.

References

[1] K. Hachem, D. Bokov, M.D. Farahani, B. Mehdizade, A.A.K. Farizhandi, Ultrasound-assisted adsorption of dyes and cadmium ion from aqueous solutions by $ZnAl_2O_4$ nanoparticles, Mater. Chem. Phys. 276 (2022), 125398.

[2] M. Alizadeh, S.J. Peighambardoust, R. Foroutan, H. Azimi, B. Ramavandi, Surface magnetization of hydrolyzed luffa Cylindrica biowaste with cobalt ferrite nanoparticles for facile Ni^{2+} removal from wastewater, Environ. Res. 212 (2022), 113242.

[3] T. Liu, Y. Lawluvy, Y. Shi, J.O. Ighalo, Y. He, Y. Zhang, P.-S. Yap, Adsorption of cadmium and lead from aqueous solution using modified biochar: a review, J. Environ. Chem. Eng. 10 (1) (2022), 106502, https://doi.org/10.1016/j.jece.2021.106502.

[4] X. Li, Z. Shi, J. Zhang, T. Gan, Z. Xiao, Aqueous Cr (VI) removal performance of an invasive plant-derived biochar modified by mg/Al-layered double hydroxides, Colloid Interface Sci. Commun. 53 (2023), 100700, https://doi.org/10.1016/j.colcom.2023.100700.

[5] J. Wang, T. Wang, Q. Zhu, S. Zhang, Q. Shi, J.-M. Chovelon, H. Wang, Preparation of a novel sludge-derived biochar by K_2FeO_4 conditioning to enhance the removal of Pb^{2+}, Colloid Interface Sci. Commun. 42 (2021), 100417 https://doi.org/10.1016/j.colcom.2021.100417.

[6] J.F. Chin, Z.W. Heng, H.C. Teoh, W.C. Chong, Y.L. Pang, Recent development of magnetic biochar crosslinked chitosan on heavy metal removal from wastewater – modification, application and mechanism, Chemosphere 291 (2022), 133035, https://doi.org/10.1016/j.chemosphere.2021.133035.

[7] Y. Zhang, Y. Wang, Z. Zhang, W. Cui, X. Zhang, S. Wang, Removing copper and cadmium from water and sediment by magnetic microspheres - $MnFe_2O_4$/chitosan prepared by waste shrimp shells, J. Environ. Chem. Eng. 9 (1) (2021), 104647, https://doi.org/10.1016/j.jece.2020.104647.

[8] H.E. Emam, M. El-Shahat, M. Taha, R.M. Abdelhameed, Microwave assisted post-synthetic modification of IRMOF-3 and MIL-68-NH_2 onto cotton for fuel purification with computational explanation, Surf. Interfaces 30 (2022), 101940, https://doi.org/10.1016/j.surfin.2022.101940.

[9] H.A. Kiwaan, F.Sh. Mohamed, A.A. El-Bindary, N.A. El-Ghamaz, H.R. Abo-Yassin, M.A. El-Bindary, Synthesis, identification and application of metal organic framework for removal of industrial cationic dyes, J. Mol. Liq. 342 (2021), 117435, https://doi.org/10.1016/j.molliq.2021.117435.

[10] H.E. Emam, R.M. Abdelhameed, H.B. Ahmed, Adsorptive performance of MOFs and MOF containing composites for clean energy and safe environment, J. Environ. Chem. Eng. 8 (5) (2020), 104386, https://doi.org/10.1016/j.jece.2020.104386.

[11] E. Moumen, S. El Hankari, MOF-assisted synthesis of mesoporous zirconium phosphate for enhanced cadmium removal from water, Colloid Interface Sci. Commun. 52 (2023), 100691, https://doi.org/10.1016/j.colcom.2022.100691.

[12] H.A. Kiwaan, F.Sh. Mohamed, N.A. El-Ghamaz, N.M. Beshry, A.A. El-Bindary, Experimental and electrical studies of zeolitic imidazolate framework-8 for the adsorption of different dyes, J. Mol. Liq. 338 (2021), 116670, https://doi.org/10.1016/j.molliq.2021.116670.

[13] R. Foroutan, S.J. Peighambardoust, M. Amarzadeh, A.K. Korri, N. S. Peighambardoust, A. Ahmad, B. Ramavandi, Nickel ions abatement from aqueous solutions and shipbuilding industry wastewater using ZIF-8-chicken beak hydroxyapatite, J. Mol. Liq. 356 (2022), 119003.

[14] H.E. Emam, R.M. Abdelhameed, Separation of anthocyanin from roselle extract by cationic nano-rode ZIF-8 constructed using removable template, J. Mol. Struct. 1267 (2022), 133607, https://doi.org/10.1016/j.molstruc.2022.133607.

[15] S. Yuan, J. Zhang, Z. Tan, Adsorption effect and the removal mechanism of silicate composite biochar particles on cadmium in soil, Chemosphere 303 (2022), 134970, https://doi.org/10.1016/j.chemosphere.2022.134970.

[16] R. Janu, V. Mrlik, D. Ribitsch, J. Hofman, P. Sedláček, L. Bielská, G. Soja, Biochar surface functional groups as affected by biomass feedstock, biochar composition and pyrolysis temperature, Carbon Resour. Convers. 4 (2021) 36–46.

[17] D. Chen, X. Yu, C. Song, X. Pang, J. Huang, Y. Li, Effect of pyrolysis temperature on the chemical oxidation stability of bamboo biochar, Bioresour. Technol. 218 (2016) 1303–1306.

[18] A. Modi, Z. Jiang, R. Kasher, Hydrostable ZIF-8 layer on polyacrylonitrile membrane for efficient treatment of oilfield produced water, Chem. Eng. J. 434 (2022), 133513.

[19] R. Foroutan, R. Mohammadi, A. Ahmadi, G. Bikhabar, F. Babaei, B. Ramavandi, Impact of ZnO and Fe_3O_4 magnetic nanoscale on the methyl violet 2B removal efficiency of the activated carbon oak wood, Chemosphere 286 (2022), 131632.

[20] R. Gurav, S.K. Bhatia, T.-R. Choi, Y.-K. Choi, H.J. Kim, H.-S. Song, S.M. Lee, S. L. Park, H.S. Lee, J. Koh, Application of macroalgal biomass derived biochar and bioelectrochemical system with Shewanella for the adsorptive removal and biodegradation of toxic azo dye, Chemosphere 264 (2021), 128539.

[21] R. Foroutan, S.J. Peighambardoust, P. Latifi, A. Ahmadi, M. Alizadeh, B. Ramavandi, Carbon nanotubes/β-cyclodextrin/$MnFe_2O_4$ as a magnetic nanocomposite powder for tetracycline antibiotic decontamination from different aqueous environments, J. Environ. Chem. Eng. 9 (6) (2021), 106344.

[22] X. Jin, C. Wu, X. Tian, P. Wang, Y. Zhou, J. Zuo, A magnetic-void-porous $MnFe_2O_4$/carbon microspheres nano-catalyst for catalytic ozonation: preparation, performance and mechanism, Environ. Sci. Ecotechnol. 7 (2021), 100110.

[23] A. Esmaeili, S. Ghobadianpour, Vancomycin loaded superparamagnetic $MnFe_2O_4$ nanoparticles coated with PEGylated chitosan to enhance antibacterial activity, Int. J. Pharm. 501 (1–2) (2016) 326–330.

[24] P. Hidalgo, R. Navia, R. Hunter, G. Coronado, M. Gonzalez, Synthesis of carbon nanotubes using biochar as precursor material under microwave irradiation, J. Environ. Manag. 244 (2019) 83–91.

[25] N. Gugin, J.A. Villajos, I. Feldmann, F. Emmerling, Mix and wait–a relaxed way for synthesizing ZIF-8, RSC Adv. 12 (15) (2022) 8940–8944.

[26] C. Cárdenas-Ramírez, F. Jaramillo, A.G. Fernández, L.F. Cabeza, M.A. Gómez, Influence of thermal treatments on the absorption and thermal properties of a clay mineral support used for shape-stabilization of fatty acids, J. Energy Storage 36 (2021), 102427.

[27] H.R. Amedi, M. Aghajani, Aminosilane-functionalized ZIF-8/PEBA mixed matrix membrane for gas separation application, Microporous Mesoporous Mater. 247 (2017) 124–135.

[28] C. Yuan, A.E.-F. Abomohra, S. Wang, Q. Liu, S. Zhao, B. Cao, X. Hu, F. Marrakchi, Z. He, Y. Hu, High-grade biofuel production from catalytic pyrolysis of waste clay oil using modified activated seaweed carbon-based catalyst, J. Clean. Prod. 313 (2021), 127928.

[29] M. Kavand, P. Eslami, L. Razeh, The adsorption of cadmium and lead ions from the synthesis wastewater with the activated carbon: optimization of the single and binary systems, J. Water Process Eng. 34 (2020), 101151.

[30] R. Foroutan, R. Mohammadi, S. Farjadfard, H. Esmaeili, B. Ramavandi, G.A. Sorial, Eggshell nano-particle potential for methyl violet and mercury ion removal: surface study and field application, Adv. Powder Technol. 30 (10) (2019) 2188–2199.